Manifestations of Broken Symmetry: The Surface Phases of $Ca_{2-x}Sr_xRuO_4$

R. G. Moore,[1] V. B. Nascimento,[1] Jiandi Zhang,[2,3] J. Rundgren,[4] R. Jin,[3] D. Mandrus,[3] and E. W. Plummer[1,3,5]

[1]*Department of Physics and Astronomy, University of Tennessee, Knoxville, Tennessee 37996, USA*
[2]*Department of Physics, Florida International University, Miami, Florida 33199, USA*
[3]*Materials Science and Technology Division, Oak Ridge National Laboratory, Oak Ridge, Tennessee 37831, USA*
[4]*Department of Theoretical Physics, Alba Nova Research Center, Royal Institute of Technology (KTH), SE-106 91 Stockholm, Sweden*
[5]*Center for Nanophase Materials Sciences, Oak Ridge National Laboratory, Oak Ridge, Tennessee 37831, USA*

(Received 14 September 2007; published 13 February 2008)

The surface structural phases of $Ca_{2-x}Sr_xRuO_4$ are investigated using quantitative low energy electron diffraction. The broken symmetry at the surface enhances the structural instability against the RuO_6 rotational distortion while diminishing the instability against the RuO_6 tilt distortion occurring within the bulk crystal. As a result, suppressed structural and electronic surface phase transition temperatures are observed, including the appearance of an inherent Mott metal-to-insulator transition for $x = 0.1$ and possible modifications of the surface quantum critical point near $x_c \sim 0.5$.

DOI: 10.1103/PhysRevLett.100.066102 PACS numbers: 68.35.B−, 61.05.jh, 71.30.+h, 74.70.Pq

The discovery of superconductivity in Sr_2RuO_4 created a flurry of experimental and theoretical activity [1]. The structural similarity with La_2CuO_4, the parent compound of the superconducting cuprates, combined with the nonconventional p-wave superconducting order parameter makes Sr_2RuO_4 a focus of intense investigation [2]. The substitution of Ca^{2+} for Sr^{2+} yields a phase diagram similar to the high-T_c cuprates, thus offering another opportunity to study the ground state evolution from an antiferromagnetic Mott insulator to a superconductor [3–5]. One advantage of the $Ca_{2-x}Sr_xRuO_4$ (CSRO) compounds is isovalent substitution between Ca^{2+} and Sr^{2+} which alters structural, electronic and magnetic properties by tuning lattice distortions. Numerous theoretical and experimental works reveal the intricate coupling of the RuO_6 structural distortions with the electronic and magnetic degrees of freedom [3–11]. Another advantage is that CSRO is a layered perovskite compound; thus, its crystals are amenable to cleaving. As such, the study of a pristine [0 0 1] surface is possible through *in situ* cleaving under ultra high vacuum conditions, thus allowing an opportunity to investigate the intricate coupling between structure and other active degrees of freedom in an environment of broken symmetry. In this work, the surface structural phases are determined by quantitative analysis of low energy electron diffraction (LEED I-V) spectra and compared to bulk studies [12,13].

The bulk structural phases of the CSRO family have been previously determined by x-ray and neutron scattering utilizing both powder and single crystal samples [5,6,14,15]. Starting from the highly symmetric $I4/mmm$ symmetry (no RuO_6 tilt or rotation) of Sr_2RuO_4 shown in Fig. 1, the smaller Ca^{2+} cation shrinks the unit cell volume while the RuO_6 volume remains fairly constant. The shrinking cage surrounding the octahedron induces a chemical pressure rotating the RuO_6 into an $I4_1/acd$ symmetry while maintaining a uniform octahedral shape and volume for $0.5 \leq x \leq 1.5$. When $x < 0.5$, an octahedral tilt is induced entering into an orthorhombic $Pbca$ symmetry. For $0.2 \leq x < 0.5$, a temperature (T)-dependent second order phase transition is observed with no hysteresis [5]. For Sr_2RuO_4, the system instability against the rotational distortion is illustrated by a softening of the RuO_6 rotational Σ_3 phonon mode [16]. A similar structural instability for $x \sim 0.5$ is characterized by a softening of the RuO_6 tilting Σ_4 phonon mode [17]. Both the $I4_1/acd$ and $Pbca$ phases can be viewed as arising from the freezing of the Σ_3 and Σ_4 modes, respectively. For $x < 0.2$ the system is always found in the $Pbca$ phase [5]. Across the metal-to-insulator transition (MIT) for $x < 0.2$ a structural phase transition is encountered described by a flattening of the RuO_6 and larger lattice distortions. While the bulk sym-

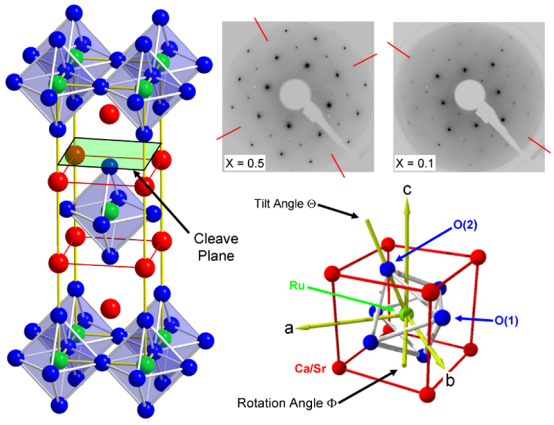

FIG. 1 (color online). Left: Bulk $I4/mmm$ structure of Sr_2RuO_4. Top Middle: LEED pattern for $x = 0.5$ showing $p4gm$ plane group symmetry. Glide lines (on which fraction spots are extinct) are emphasized by red lines. Top Right: LEED pattern for $x = 0.1$ showing pg symmetry with only one glide line. Bottom right: Structural parameters used in describing bulk and surface geometries.

metry does not change across the MIT, the Ru-O(2) oxygen bond lengths decrease ~0.05 Å while the Ru-O(1) bond lengths increase ~0.05 Å. In addition, the tilt of the RuO_6 increases ~5° on average [5]. The structural distortions yield a smaller c/a axis ratio in the insulating phase while the volume of the RuO_6 increases ~3%.

High quality single crystals were grown using the optical floating zone technique. All crystals were well characterized and concentrations verified by energy dispersive x-ray analysis. Crystals were cleaved and measured *in situ* with a base pressure of 8×10^{-11} torr revealing pristine [001] surfaces with large micrometer terraces observed by STM. While it has been shown previously that the surface of Sr_2RuO_4 reconstructs to form a lower symmetry [18], for $x \leq 1.5$ the crystals reveal a $p(1 \times 1)$ surface as shown in Fig. 1. All available beams were collected at normal incidence and symmetrically averaged yielding 16 nonequivalent beams for $x = 0.1$ and 11 nonequivalent beams for $0.2 \leq x \leq 2.0$. Total I-V energy ranges varied slightly from surface to surface but all I-V sets were >3000 eV with the majority being >3700 eV. Theoretical I-V curves generated for structural refinements employed a modified version of the SATLEED program described elsewhere [19,20]. Because of the glide plane symmetry, simulated annealing optimization algorithms were written taking advantage of bulk space group symmetry generators tailored for each surface [21]. In addition, the performance of the simulated annealing algorithms was checked by manual grid searches for a few concentrations. Additional fit parameters were included to account for possible asymmetric c-axis displacements that do not destroy the observed $p(1 \times 1)$ LEED pattern. The Pendry reliability factor (R_p) was used as a measure of agreement between theory and experiment [22]. For all surfaces studied the refined surface structures yielded $0.19 \leq R_p \leq 0.28$ indicating excellent agreement between theory and experiment.

All $0.2 \leq x \leq 2.0$ samples cleaved at room temperature (RT) exhibit a $p4gm$ plane group symmetry. The glide lines presented in Fig. 1 are due to the rotation of the RuO_6 about an axis parallel to the c-axis. While the expected symmetry for a bulk terminated $I4_1/acd$ surface ($0.2 \leq x \leq 1.5$) is $p2gg$, multiple terrace terminations generate the $p4gm$ symmetry [20]. For $x < 0.2$, a pg plane group symmetry is revealed, also shown in Fig. 1, reflecting the symmetry of the bulk terminated $Pbca$ structure. The $Pbca$ symmetry is generated from a rotation plus a tilt of the RuO_6. The tilt destroys one of the glide lines and thus only one is evident in the LEED pattern shown in Fig. 1.

The surface structures for the entire series at RT have been determined and the results are presented in Fig. 2. For $x > 1.5$, the bulk symmetry is $I4/mmm$, however, no surface analog to the $I4/mmm$ symmetry ($P4mm$) is observed for any concentration. The surface stabilizes the bulk instability against the RuO_6 rotational distortion [5],

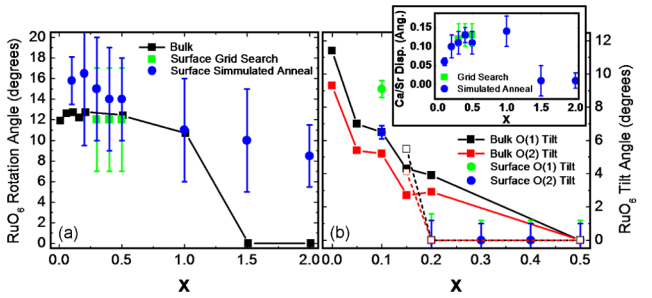

FIG. 2 (color online). (a) Bulk and surface RuO_6 rotation angle versus concentration at $T = 300$ K. The surface equivalent of a bulk terminated $I4/mmm$ symmetry never exists as a RuO_6 rotation exists for all x. (b) Bulk and Surface RuO_6 tilt angles versus concentration. The solid lines (filled squares) represent bulk powder data while the dashed lines (open squares) represent bulk single crystal data [5,15]. The critical tilt concentration is $x = 0.2$ for both bulk and surface single crystals. Tilt angles are slightly enhanced for $x = 0.1$. Inset shows the inward Ca/Sr displacement for different x. Vertical lines show transition from $p4gm$ to pg symmetry.

freezing in the soft zone-boundary Σ_3 phonon mode creating a single $p4gm$ phase from $0.2 \leq x \leq 2.0$. The surface RuO_6 tilt angles at RT shown in Fig. 2(b) are more akin to bulk trends as no RuO_6 tilt is encountered for $x \geq 0.2$, similar to bulk single crystal data [5,15]. The tilts encountered for the $x = 0.1$ metallic phase are larger than those values encountered in the bulk metallic phase, but are smaller than the bulk insulating phase. The largest surface relaxation observed on the CSRO surface involves the topmost Ca/Sr ions where a significant inward motion is encountered for $x \leq 1.0$ as shown in the Fig. 2(b) inset. The RT structure for $0.2 \leq x \leq 1.0$ shows a large 0.1 Å Ca/Sr inward motion but for $x = 0.1$, where a tilt already exists, the inward motion is only 0.06 Å. A simple electrostatic argument would indicate that when the surface is formed the topmost Ca/Sr-O(2) layer would be forced down [23], but the insert in Fig. 2(b) shows that it is not that simple. The surface buckling increases and is intimately tied to the stability of the RuO_6 tilt. While one might expect the creation of a surface to accentuate the system instability against the tilt distortion, the observed trend discussed below indicates the RuO_6 tilt is stabilized by the creation of a surface.

The RT LEED pattern for $0.2 \leq x \leq 2.0$ is shown in Fig. 1. The glide lines of the $p4gm$ symmetry is evident by the extinguished $(\pm h, 0)$ and $(0, \pm h)$ spots where h is an odd integer. To investigate the surface high temperature tetragonal-to-low temperature orthorhombic (HTT-LTO) phase transition, crystals were cleaved at RT and subsequently cooled. As the $Pbca$ bulk phase boundary is traversed the tilting RuO_6 octahedral destroys the glide line symmetry resulting in the appearance of the $(h, 0)$ beams. One would expect the low temperature LEED pattern to be similar to that of $x = 0.1$. However, such is

not the case as both the $(h, 0)$ and $(0, h)$ beams are evident in the LTO LEED pattern revealing a *pm* plane group symmetry.

Using integrated (0,3) and (3,0) beam intensity at $E_i = 176$ eV as an order parameter, the surface HTT-LTO phase boundary is determined. As the system is cooled, broad diffuse (0,3) and (3,0) beams become evident for $0.2 < x \leq 0.5$, indicated in Fig. 3 and 4 by a temperature T^*. Such diffuse beams are typical of short-range correlations similar to those observed in neutron data [5,15]. In contrast to neutron studies, the beam intensity is nearly constant for a considerable temperature range indicating the system instability against the tilt distortion but never achieving the *Pbca* phase. As the phase boundary is traversed, the beam intensity dramatically increases and the beam size shrinks as long range order is established. The behavior of both sets of beams is similar across the phase boundary and beam intensity is the only difference as shown in Fig. 3. The normalized order parameter intensity across the phase boundary for $x = 0.3$ is shown in Fig. 3(a) revealing $T_c \sim 170$ K, some 20 K below the bulk value [24]. While previous bulk studies demonstrate the lack of hysteresis indicating a second order nature for the bulk phase transition [5,17], a ~10 K hysteresis is observed on the surface. The doping dependence for T_c has been evaluated for $0.2 \leq x < 0.5$ ($x = 0.2$, 0.3, 0.4, and 0.5) and the general trend is similar to $x = 0.3$: the surface T_c is suppressed from bulk values and a hysteresis is always observed. T^* is typically larger than the bulk transition temperature. The general behavior of this surface phase transition is displayed in Fig. 4.

For $x < 0.2$ a doping-dependent metal-to-insulator transition exists. Upon cooling, a Mott transition occurs between a paramagnetic metal and an antiferromagnetic insulator. In the bulk, the transition is coupled to a structural phase transition [3,5,6]. While the structural phases for larger values of x can be described by rotations and tilts of a rigid RuO_6 octahedron, it is found that in the insulating state, the octahedron is flattened. The flattening octahedron

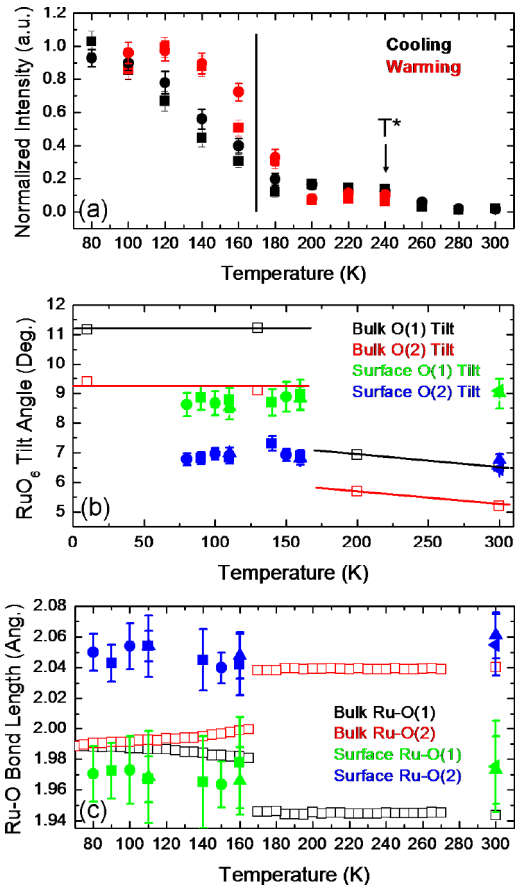

FIG. 3 (color online). (a) HTT-LTO phase transition order parameter for $x = 0.3$ showing first order phase transition character with hysteresis. The solid squares are the integrated beam (0,3) intensity at 176 eV normalized to the beam (2,2) intensity at 115 eV. The solid circles are the normalized beam (3,0) intensity. Vertical line shows transition from *p*4*gm* to *pm* symmetry while arrow shows the onset of the tilt instability (T^*). (b) Surface RuO_6 tilt angles for $x = 0.1$ across bulk and surface MITs. The four closed symbols represent four different crystal surfaces studied. The bulk data (open symbols) are shown for comparison with lines as guides to the eye. The bulk data are from neutron powder experiments with a $T_c \sim 170$ K [5] while T_c in our bulk single crystals is 154 K. The surface MIT $T_c = 130$ K [23]. (c) Surface Ru-O bond lengths for $x = 0.1$ across bulk and surface MITs. Neither the RuO_6 tilts nor the Ru-O bond lengths show evidence (within experimental error) of a structural phase transition across the surface MIT.

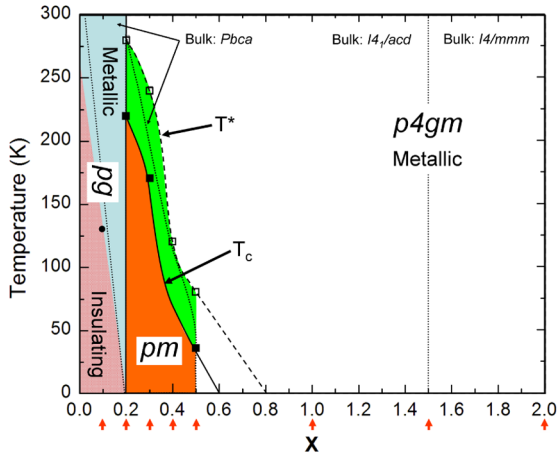

FIG. 4 (color online). Surface phase diagram for $Ca_{2-x}Sr_xRuO_4$. The dashed T^* line is the temperature where a tilt instability is revealed by weak diffuse reflections and the solid T_c line is the *p*4*gm*-*pm* structural phase boundary. The dotted lines represent bulk structural phase transitions [5,15,17,24]. There is no solid line between the metallic and insulating phases for $x < 0.2$ as no structural phase transition exists across the surface MIT. Red arrows indicate different concentrations investigated in this study. The unshaded regions below the solid and dashed lines for $0.5 \leq x \leq 0.8$ are extrapolations based on observed surface trends.

across the MIT is characterized by a sharp decrease of the Ru-O(2) bond lengths and increased tilts. On the surface, previous studies have shown the surface MIT T_c to be $\sim$20 K lower than the corresponding bulk value for $x = 0.1$ and it is imperative to understand the role of surface structure across the phase boundary [23]. Figures 3(b) and 3(c) reveal striking deviations between surface and bulk behavior, the surface structure across the MIT does not change. While the RuO_6 tilt increases, it does not increase to those values encountered in the insulating bulk. In addition, the Ru-O(1) basal plane and Ru-O(2) apical bond lengths, as well as all other structural parameters, remain static through the phase transition. A 3.3% increase in RuO_6 volume is encountered due to a $\sim 4^\circ$ increase in RuO_6 rotation on the surface. While it has been argued that the structural distortions across the bulk Mott MIT are responsible for the electron localization [10,11], the surface MIT is not coupled to any structural phase transition and is purely electronic in character, i.e., *inherent* [23].

Lower HTT-LTO transition temperatures and the lack of a structural distortion across the surface MIT suggest the tilt is stabilized on the surface. In addition, LDA calculations reveal the inward motion of the Ca/Sr plane interferes with the tilting of the RuO_6 across the $x = 0.1$ MIT [23]. The general trend suggests the inward motion of the topmost Ca/Sr ions plays a significant role in both the static tilt across the MIT for $x = 0.1$ and the suppressed HTT-LTO phase boundary for $0.2 \leq x < 0.5$. The inward motion of the top Ca/Sr ions creates a compression stress which interferes with the RuO_6. Theoretical calculations suggest a similar surface compression should exist on other perovskite material surfaces but experimental evidence has been lacking [25,26]. The observed CSRO surface trends would suggest the $x_c = 0.5$ bulk quantum critical point (QCP) should be shifted to lower x on the surface. However, initial results near the QCP reveal the surface phases to be more complex. While bulk studies reveal the HTT-LTO $T_c = 155$ K for $x = 0.4$ [17], a significant surface suppression of the RuO_6 tilt is encountered as no evidence for the HTT-LTO transition is observed down to 80 K. On the contrary, weak diffuse superstructure reflections are evident at $\sim$80 K (T^*) for $x = 0.5$ on the surface and the HTT-LTO phase boundary is revealed at $T_c \sim$ 40 K. Extrapolation of both T_c and T^* to zero in Fig. 4 shows that the broken symmetry at the surface will most likely displace or even destroy the $x_c = 0.5$ QCP at the surface. Further investigations are required to fully determine the existence and position of the QCP on the surface.

In summary, the surface structural phase diagram of $Ca_{2-x}Sr_xRuO_4$ has been determined and is presented in Fig. 4. The RT surface structural phases follow bulk trends with the exception that no $I4/mmm$ symmetry is observed on the surface for $x \geq 1.5$. Significant deviations between surface and bulk behavior are encountered across T-dependent structural phase boundaries. While the RuO_6 rotation is revealed for all x, a large inward motion of the topmost Ca/Sr ions interferes with the RuO_6 tilt. As a result, lower surface HTT-LTO transition temperatures are observed for $0.2 \leq x < 0.5$ and the surface Mott MIT T_c is suppressed for $x < 0.2$. In addition, further significant surface deviations from bulk behavior is noted as a hysteresis is observed across the surface HTT-LTO phase boundary and the structural transitions accompanying the Mott MIT in the bulk are simply nonexistent on the surface. Implications of the inward motion of the top Ca/Sr ions on the QCP at $x_c \sim 0.5$ are not yet clear as an unexpected HTT-LTO phase boundary is revealed on the surface at $T_c \sim 40$ K for $x = 0.5$.

This work was supported by DOE, Division of Materials Sciences and Engineering through ORNL. R. G. M. acknowledges support from NSF and DOE (DMS&E) (No. NSF-DMR-0451163). J. Z. is thankful for the support from US NSF, under Contract No. DMR-0346826.

[1] Y. Maeno *et al.*, Nature (London) **372**, 532 (1994).
[2] Y. Maeno, R. Maurice, and M. Sigrist, Phys. Today **54**, 42 (2001).
[3] S. Nakatsuji and Y. Maeno, Phys. Rev. Lett. **84**, 2666 (2000).
[4] S. Nakatsuji *et al.*, Phys. Rev. Lett. **90**, 137202 (2003).
[5] O. Friedt *et al.*, Phys. Rev. B **63**, 174432 (2001).
[6] M. Braden, G. Andre, S. Nakatsuji, and Y. Maeno, Phys. Rev. B **58**, 847 (1998).
[7] S. -C. Wang *et al.*, Phys. Rev. Lett. **93**, 177007 (2004).
[8] Z. Fang, and K. Terakura, Phys. Rev. B **64**, 020509(R) (2001).
[9] Z. Fang, N. Nagaosa, and K. Terakura, Phys. Rev. B **69**, 045116 (2004).
[10] X. Dai, G. Kotliar, and Z. Fang, arXiv:cond-mat/0611075.
[11] A. Liebsch and H. Ishida, Phys. Rev. Lett. **98**, 216403 (2007).
[12] J. B. Pendry, *Low Energy Electron Diffraction* (Academic, London, 1974).
[13] M. A. Van Hove, W. H. Weingerg, and C. M. Chan, *Low Energy Electron Diffraction Experiment, Theory and Surface Structure Determination* (Springer-Verlag, Berlin, 1986).
[14] M. Braden *et al.*, Physica (Amsterdam) **273C**, 248 (1997).
[15] O. Friedt, Ph.D. thesis, Université Paris XI, 2003.
[16] M. Braden *et al.*, Phys. Rev. B **57**, 1236 (1998).
[17] R. G. Moore, Ph.D. thesis, University of Tennessee, 2006.
[18] R. Matzdorf *et al.*, Science **289**, 746 (2000).
[19] A. Barbieri and M. A. Van Hove (private communication).
[20] V. B. Nascimento *et al.*, Phys. Rev. B **75**, 035408 (2007).
[21] S. Kirkpatrick *et al.*, Science **220**, 671 (1983).
[22] J. B. Pendry, J. Phys. C **13**, 937 (1980).
[23] R. G. Moore *et al.*, Science **318**, 615 (2007).
[24] R. Jin *et al.*, arXiv:cond-mat/0112405.
[25] E. Heifets *et al.*, Phys. Rev. B **64**, 235417 (2001).
[26] S. Piskunov *et al.*, Surf. Sci. **575**, 75 (2005).